

# Direct Search for Low Mass Dark Matter Particles with CCDs

J. Barreto<sup>1</sup>, H. Cease<sup>2</sup>, H.T. Diehl<sup>2</sup>, J. Estrada<sup>2</sup>, B. Flaugh<sup>2</sup>, N. Harrison<sup>2</sup>, J. Jones<sup>2</sup>, B. Kilminster<sup>2</sup>, J. Molina<sup>3</sup>, J. Smith<sup>2</sup>, T. Schwarz<sup>4</sup> and A. Sonnenschein<sup>2</sup>

<sup>1</sup>*Universidade Federal do Rio de Janeiro (UFRJ),  
Rio de Janeiro, Brazil*

<sup>2</sup>*Fermi National Accelerator Laboratory,  
Batavia, Illinois, USA*

<sup>3</sup>*Facultad de Ingenieria,  
Universidad Nacional de Asuncion (FIUNA), Asuncion, Paraguay*

<sup>4</sup>*University of California at Davis, USA.*

(Dated: October 9, 2018)

A direct dark matter search is performed using fully-depleted high-resistivity CCD detectors. Due to their low electronic readout noise (R.M.S.  $\sim 7$  eV) these devices operate with a very low detection threshold of 40 eV, making the search for dark matter particles with low masses ( $\sim 5$  GeV) possible. The results of an engineering run performed in a shallow underground site are presented, demonstrating the potential of this technology in the low mass region.

PACS numbers: 93.35.+d, 95.55.Aq

## I. INTRODUCTION

There have been several direct-detection experiments searching for dark matter (DM) performed in recent years, and several more in development [1]. Most of these experiments have been optimized for detecting the elastic scattering of DM particles with masses larger than 50 GeV, concentrating on the most natural region of the Weakly Interactive Massive Particle (WIMP) parameter space such that DM corresponds to the lightest supersymmetric particle [2]. Detection thresholds of a few keV are typical for such high mass DM searches. Recent results from experiments that operate with a lower threshold [3, 4] have presented hints of a DM signal at low energies, the most notable being DAMA/Libra which claims a high-significance detection of an annual modulation [3]. More recently, the CoGeNT Collaboration has seen a possible hint for a low mass DM signal using a low threshold Ge detector [4]. Motivated by these results, new theoretical interpretations have been developed for which low thresholds are needed to directly detect DM [5–11]. In these models the DM particles are either much lighter than 50 GeV or present a non-elastic interaction with the detector nuclei [12]. Because of noise in detector electronics and efficiency issues, most experiments are not capable of significantly lowering the detection threshold to probe the new models. For this reason there is an effort by the experimental community to develop techniques that could detect low energy signals from DM [4] [13]. This work presents a DM search using Charge-Coupled Devices (CCDs) using a detection threshold of 40 eV electron equivalent energy (eVee).

CCDs used for astronomical imaging and spectroscopy commonly achieve readout noise levels of  $2 e^-$  R.M.S., equivalent to 7.2 eV of ionizing energy in Silicon. Though this allows for a very low detection threshold, these detectors have not been considered for DM searches because

of their very low fiducial mass. The recent development of thick, fully-depleted CCDs, ten times more massive than conventional CCDs, has changed the situation. The Dark Matter in CCDs (DAMIC) experiment is the first DM search to exploit this technology.

## II. HIGH RESISTIVITY CCD DETECTORS

In an effort to increase the near-IR photon detection efficiency of CCDs, a group at Lawrence Berkeley National Laboratory (LBNL) developed detectors with a depletion region up to 300  $\mu\text{m}$  thick [14]. These devices are fabricated with high resistivity silicon ( $\sim 10\text{k}\Omega\text{cm}$ ). Due to their higher efficiencies for detecting photons with red and near infrared wavelengths, these devices have been selected for astronomical instrumentation [15, 16], in particular, the Dark Energy Camera (DECam) [17, 18]. The DAMIC experiment uses DECam CCDs to search for DM.

The DECam CCDs [17, 19–21, 23] are back-illuminated, p-channel CCDs thinned to 250  $\mu\text{m}$  and biased with 40 V from the back side to achieve full depletion. The positively-charged holes produced in the depletion region are stored in the buried channels, a few  $\mu\text{m}$  away from the the gate electrodes. Charge produced near the back surface must travel the full thickness of the device to reach the potential well. During this transit inside the depletion region, a hole could also move in the direction perpendicular to the pixel boundaries. This effect, called charge diffusion, must be regulated to avoid a significant degradation in image quality. The CCDs used in most astronomical instruments are thinned to  $< 40 \mu\text{m}$  to reduce charge diffusion. For the DECam CCDs, a substrate voltage is applied to the back surface to control diffusion and obtain acceptable image quality.

The two main features that make the DECam CCDs

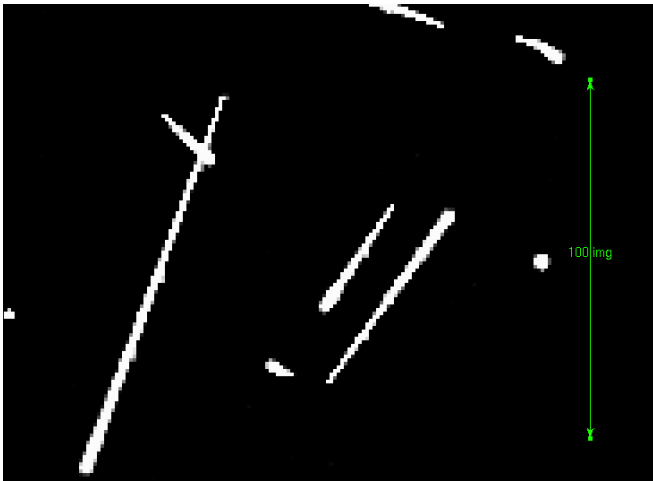


FIG. 1: Four muons tracks are clearly reconstructed on this image. There is a significant width different between the two ends of the track. The thicker end corresponds to the region of the track in the back of the CCD, with maximum diffusion. The thinner end corresponds to the front of the CCD. The smaller circular hits are diffusion-limited hits as expected for nuclear recoils. The line is 100 pixels long and was added to give a sense of scale.

good candidates for a direct dark matter search are their thickness, which allows the CCD to have significant mass, and the low electronic readout noise, which permits a very low energy threshold for the ionization signal produced by nuclear recoils.

DAMIC uses a single rectangular CCD readout with a Monsoon controller [22]. The detectors have 4.2 million pixels with dimensions  $15 \mu\text{m} \times 15 \mu\text{m}$  (active mass of 0.5 g), and are read by two amplifiers in parallel. The detectors have an output stage with an electronic gain of  $\sim 2.5 \mu\text{V}/e$ . The signal is digitized after correlated double sampling (CDS) and the noise performance depends on the readout speed. The best noise,  $\sigma < 2e^-$  (R.M.S.) per pixel, was achieved with readout times of  $50 \mu\text{s}$  per pixel [19–21, 23].

### III. CCD CALIBRATION: X-RAYS AND NUCLEAR RECOILS

X-rays are commonly used in the energy calibration of CCD detectors [24]. X-rays from  $^{55}\text{Fe}$  penetrate only  $\sim 20 \mu\text{m}$  into the silicon before producing charge pairs according to the well known conversion factor of  $3.64 \text{ eV}/e^-$  [24]. As a result of this process X-rays produce hits in the detector with size limited by charge diffusion. In a back illuminated DECam CCD the size of the 5.9 keV X-rays is  $\sim 7.5 \mu\text{m}$  R.M.S. [25]. Using processing tools developed for astronomical applications [26], the X-ray hits are identified in the CCD images as reconstructed charge clusters with a size limited by diffusion. Fig. 1 shows

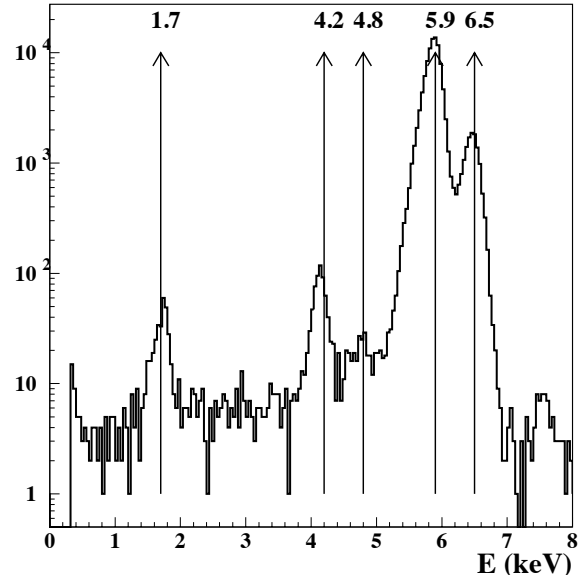


FIG. 2: Spectrum obtained for the reconstructed X-ray hits in an  $^{55}\text{Fe}$  exposure of a DECam CCD. The arrows mark the direct X-rays from the source:  $K\alpha=5.9 \text{ keV}$  and  $K\beta=6.5 \text{ keV}$ , their escape lines at 4.2 and 4.8 keV [24], and the Si X-ray at 1.7 keV. The factor  $3.64 \text{ eV}/e^-$  is used to convert from charge to ionization energy. The feature at 7.6 keV is consistent with pixels that hit by a 5.9 keV and a 1.7 keV X-ray on the same exposure. consistent w

two examples of diffusion-limited hits. The energy of the X-ray hit is proportional to the charge collected in all the pixels that belong to this cluster. An example of the energy spectrum measured for an  $^{55}\text{Fe}$  X-ray exposure in a DECam CCD is shown in Fig. 2.

Figure 2 provides a good calibration for X-rays in silicon. Since the ionization efficiency for nuclear recoils differs from the ionization efficiency for X-rays, the results are not directly applicable to nuclear recoils expected from DM interactions. The ratio between the ionization efficiency for nuclear recoils and ionization efficiency for electron recoils is usually referred to as the quenching factor ( $Q$ ). The quenching factor has been measured in Si for recoil energies above 4 keV [27], showing good agreement with the Lindhard model [28, 29]. For recoil energies less than 4 keV, the quenching factor becomes increasingly energy-dependent and no previous measurements are available, as shown in Fig.3. In this work, the Lindhard model [28, 29] is used for converting visible (or electron equivalent) energy to recoil energy. We test this assumption by comparison to neutron data with a known energy spectrum.

In order to study  $Q$ , the DAMIC detector was exposed to a  $^{252}\text{Cf}$  neutron source (see Fig.4). Nuclear recoils produced by neutrons, similar to those expected from DM interactions, give diffusion-limited hits analogous to those

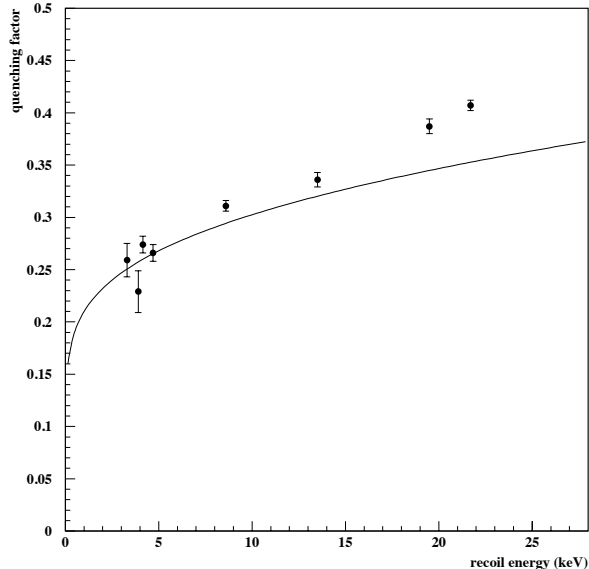


FIG. 3: Existing quenching factor measurements in Si compared with the Lindhard theory (solid line). No previous data exist for recoil energies below 4 keV[28, 29].

of X-rays. Thus, nuclear recoils in CCD images are identified by selecting diffusion-limited hits. The expected response of the detector was calculated in three steps. First neutrons were generated according to the known spectrum of the  $^{252}\text{Cf}$  source and GEANT4[30] was used to simulate the passage of these neutrons through the vacuum vessel wall housing the CCD detectors (1cm Al wall). The resulting neutron energy spectrum was then used to calculate the expected nuclear recoil in the Silicon CCD using Ref.[27]. Finally, using the ionization yield from the Lindhard theory, the expected observable energy on the CCD was calculated. The results of the simulation compared with the spectrum for diffusion-limited hits in data are shown in Fig. 5. The data shows a bump at  $\sim 1.7$  keVee consistent with Si excitations, but deviates from Lindhard model at energies below 1.5 keV. While the data appears to indicate a weaker energy dependence of the quenching factor below 1.5 keV, we use the Lindhard model in order to produce more conservative limits. For energies lower than 0.5 keV the detection efficiency for nuclear recoils has a strong energy dependence (see Fig.9) and the comparison is no longer valid. This issue will be investigated in future work.

In Fig.5 the behavior of the ionization efficiency of nuclear recoils is degenerate with the selection efficiency. The spectrum is also contaminated with electron recoils produced from the gammas generated in the  $^{252}\text{Cf}$  source. The comparison between data and simulation is also influenced by the neutron input spectrum and the simulation geometry. For these two reasons the analysis dis-

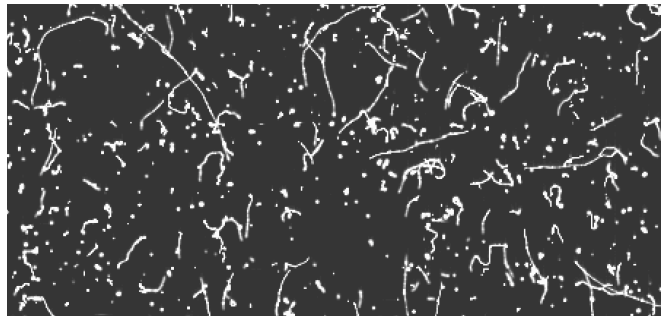


FIG. 4: Image resulting from an exposure of a DECam CCD to a  $^{252}\text{Cf}$  neutron source. The total width of the image corresponds to 1000 pixels. The smaller dots represent the diffusion-limited hits, the trails correspond to scattered electrons and there is one bigger circular cluster of charge that corresponds to an alpha particle.

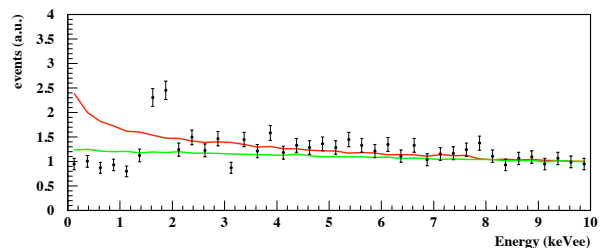


FIG. 5: Reconstructed electron equivalent energy spectrum for  $^{252}\text{Cf}$  exposures. The data is consistent with expectations from Lindhard theory (red). The expectations for an energy independent quenching factor are also shown for comparison (green).

cussed above, and summarized in Fig.5, does not constitute a measurement of  $Q$ . It should be interpreted as a comparison between the data and Lindhard model assuming a constant detection efficiency. It is presented here to illustrate the effect of energy dependent  $Q$  in the recoil spectrum and to motivate the need for a full calibration of nuclear recoils in Si at low energies.

#### IV. SELECTION OF DARK MATTER CANDIDATE EVENTS

Three selection cuts are used to separate the dark matter candidates in our images from background and noise hits. The first step requires the total energy deposited to be larger than 0.04 keVee. This cut is mostly used to suppress the noise on the readout of the CCD detector. In order to select diffusion-limited hits produced in the bulk of the CCD and not near the front or back surfaces, we impose additional two selection described below.

X-rays produce diffusion-limited hits similar to nuclear recoils in silicon, becoming an important background for a dark matter search. However, unlike nuclear recoils, the low energy X-ray photons only penetrate a few microns into the detector, producing charge very close to the back or front surfaces of the CCD. When performing a DM search it is convenient to reject hits produced near the front and back surfaces of the CCD.

Hits on the front surface will have negligible diffusion because they are produced next to the gates. Hits on the back surface have the maximum diffusion since the path is the longest to the electrodes. The dependence of diffusion with depth can be clearly seen in tracks identified as cosmic ray muons in Fig. 1. The diffusion measured for each hit becomes indicative of the depth of the hit inside the detector.

For each hit reconstructed on the CCD image the first order moments of the charge distribution along each axis are calculated, namely  $\hat{x}$  and  $\hat{y}$ . These values are an estimation of the real position of the hit on the CCD coordinates,  $x$  and  $y$ . The second order moments along both axes are also calculated as  $\hat{\sigma}_x^2$  and  $\hat{\sigma}_y^2$ , providing an estimation for the charge spread  $\sigma_x^2$  and  $\sigma_y^2$ . These four estimators are the basis of the selection cuts used to eliminate the events near the front and back surface. In the following discussion units of pixel and pixel<sup>2</sup> are implicit when presenting values for  $\hat{x}$  and  $\hat{\sigma}_x^2$ .

Unfortunately, because of the pixelation of the detectors there is a non trivial relation between the real values of  $x, y, \sigma_x^2, \sigma_y^2$  and the estimators  $\hat{x}, \hat{y}, \hat{\sigma}_x^2, \hat{\sigma}_y^2$  discussed above. For example, events close to the boundary of the pixel necessarily have  $\hat{\sigma}_x^2 > \sigma_x^2$ . At the same time, events with small charge spread  $\sigma_x^2$  tend to have  $\hat{x}$  biased towards the center of a pixel. Also due to pixelation, there is a strong correlation between  $\hat{\sigma}_x^2$  and  $\hat{x}$ , given by

$$\begin{aligned} \hat{\sigma}_x^2 &\geq 0.25 - \hat{x}^2 & \text{for } 0.0 < \hat{x} < 0.5 \text{ and} \\ \hat{\sigma}_x^2 &\geq 0.25 - (\hat{x} - 1)^2 & \text{for } 0.5 < \hat{x} < 1.0 \end{aligned} \quad (1)$$

With  $\hat{x} = 0.0$  corresponding to the edge of the pixel and  $\hat{x} = 0.5$  the center of the pixel. A similar relation applies for the  $y$ -axis.

A simulation was performed to illustrate the pixelation effects on  $\hat{x}$  and  $\hat{\sigma}_x^2$ . The simulation consisted of generating point-like charge distributions in a 250  $\mu\text{m}$  thick CCD with  $15 \times 15 \mu\text{m}^2$  pixels. Lateral diffusion for each hit was calculated as a function of the distance of the hit to the front surface (maximum diffusion was 7.5  $\mu\text{m}$  for hits 250  $\mu\text{m}$  away from the front). The results shown in Fig. 6 clearly indicate that the larger  $\hat{\sigma}_x^2$  is measured for events on the back of the detector, and that events on the front surface are very close to the curve defined by Eq.(1).

The results for  $\hat{x}$  and  $\hat{\sigma}_x^2$  with X-rays data on the front and back of the detector and shown in Fig.7, together with data from a  $^{252}\text{Cf}$  neutron source. The data shows consistency with the simulation.

Based on the discussion above, the second step for the selection of DM candidate hits consists of requiring the

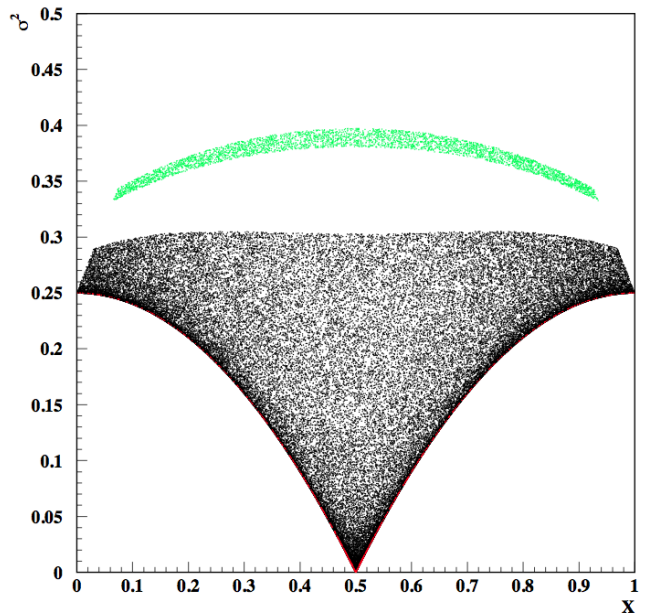


FIG. 6: Results of a simulation of charge diffusion inside a CCD. The horizontal axis shows the position of the hit inside the pixel, with  $\hat{x}=0.5$  corresponding to the center of the pixel. The vertical axis shows the size of the reconstructed hit,  $\hat{\sigma}_x^2$  in units of pixel<sup>2</sup> as defined in the text. The red points correspond to hits generated in the first 50  $\mu\text{m}$  adjacent to the front of the detector, the green points correspond to the hits generated less than 10  $\mu\text{m}$  away to the back of the CCD. The black points correspond to hits generated between 50 and 200  $\mu\text{m}$  from the front of the detector. The simulation shows that the selection criteria discussed in Eq.(2) and Eq.(3) rejects most events next to the front and back surfaces of the CCD.

charge to be distributed in more than one pixel. This is used to reject X-rays in the front surface of the detector.

The third selection cut is designed to keep hits in the bulk of the CCD while rejecting events close to the front and back surfaces of the detector. This is done in two steps, the requirement

$$\begin{aligned} \hat{\sigma}_x^2 - (0.25 - \hat{x}^2) &> 0.05 & \text{for } 0.0 < \hat{x} < 0.5 \text{ and} \\ \hat{\sigma}_x^2 - (0.25 - (1 - \hat{x})^2) &> 0.05 & \text{for } 0.5 < \hat{x} < 1.0, \end{aligned} \quad (2)$$

is used to ensure that the selected events are away from the front of the detector. To select events away from the back of the detector one additional condition is added

$$\hat{\sigma}_x^2 < 0.28 \quad (3)$$

Identical cuts are applied to the  $y$ -axis variables.

The efficiency for nuclear recoils passing the selection is estimated using  $^{252}\text{Cf}$  exposures. The reconstructed spectrum with and without the selection is shown in Fig.8. The raw spectrum (without size selection) is contaminated by low energy photons and electrons that produce a steep raise below 0.5 keV. This contamination is also evident in the image shown in Fig.4. Nuclear recoils

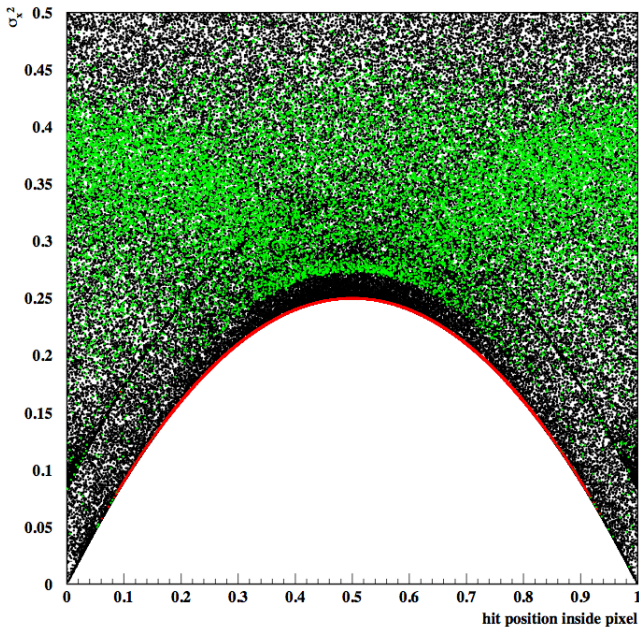


FIG. 7: Results of  $\hat{x}$  and  $\hat{\sigma}_x^2$  for 5.9 keV X-rays on front (red) and back (green) of a CCD. The black data corresponds to hits from the same  $^{252}\text{Cf}$  source shown in Fig.4. As expected from simulations the back illuminated X-rays produce hits with large  $\hat{\sigma}_x^2$ , while the front illuminated X-rays are very close to the boundary defined by Eq.1.

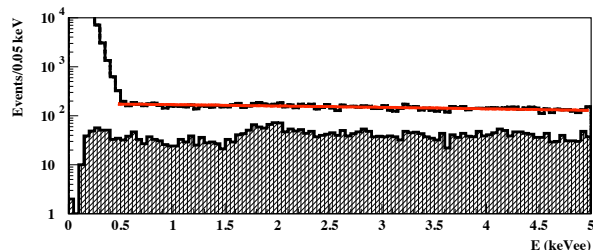


FIG. 8: Measured spectrum for  $^{252}\text{Cf}$ . The upper line shown the raw data without applying any selection criteria, the lower hatched histogram shows the result after selecting hits with intermediate size. The raw data is fitted to a linear function above 0.5 keV.

from neutrons emitted by  $^{252}\text{Cf}$  are expected to produce an approximately flat spectrum at low energies. We determine the efficiency of the selection by taking the ratio of the selected hits to a linear fit to the data before selection, in the region 0.5 keV to 10 keV where the spectrum is the most consistent with a flat line (Fig. 8). The result is shown in Fig.9.

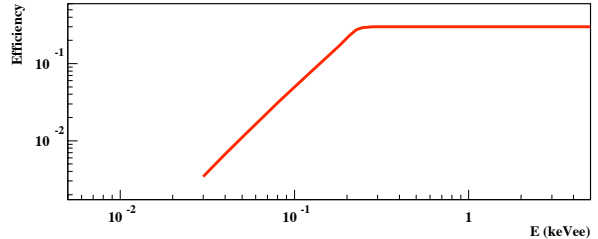


FIG. 9: Efficiency for selecting nuclear recoils with intermediate size as calculated using the data in Fig.8

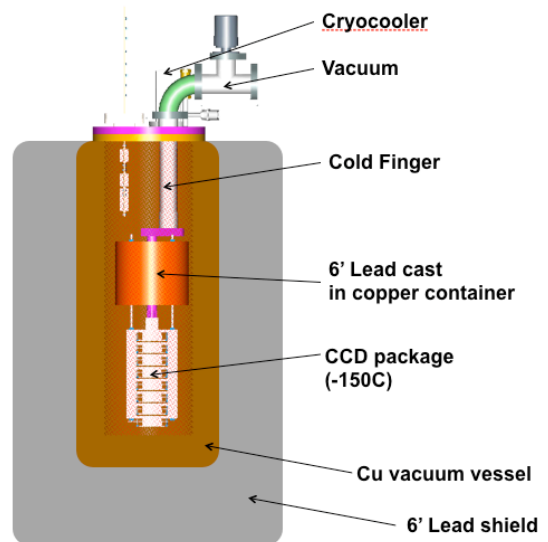


FIG. 10: Schematic of DAMIC vacuum vessel and lead shield.

## V. TEST IN SHALLOW UNDERGROUND SITE

We performed the first underground test for the use of CCDs in a direct DM search with a single 0.5 g CCD as described above. A low background CCD package was designed for this test, consisting of a readout board built on aluminum nitride (AlN) wire-bonded to the CCD with some additional AlN spacers for mechanical support. AlN is typically used in CCD packaging due to its mechanical and thermal properties and was measured to have low concentrations of radio-isotopes. The CCD package was installed inside a copper box and cooled down to -150C to reduce dark current intrinsic to the CCD. The copper box was also cooled to eliminate the infrared radiation impinging on the detector from warm surfaces. A closed cycle helium gas refrigerator [31] was used to maintain the low temperature. The detector was

TABLE I: Number of events passing selection cuts for the 107 g-day of data shown in Fig.11. two energy bins are shown: (1) from 0.04 keV to 5 keV , (2) from 0.04 keV to 15 keV.

cut	bin (1)	bin (2)
1) $E > 0.04$ keV	81754	102469
2) npixel $> 1$	26971	45353
3) hit size	433	5529

connected with a passive readout cable and the active electronic components (preamplifiers) were located outside a 6" lead shield. The detector package was housed in a cylindrical vacuum vessel fabricated with oxygen-free copper, and maintained at  $10^{-7}$  Torr by continuously running a turbo molecular pump as in Fig.10. The apparatus was installed 350' underground in the NuMI [32] near-detector hall at Fermilab, where other DM experiments have already been performed [33]. The system operates without the need of any human intervention, and was programmed to collect exposures every 40,000 seconds. The experiment operated for 11 months starting June 2010, and accumulating a total exposure of 107 g-days. The observed spectrum is shown in Fig. 11. The spectrum shows several X-ray peaks coming from known components the apparatus. It also shows three peaks at 11 keV, 12 keV and 14 keV for which the source has not been identified. The isotopic composition of the commercial cable and high density connector used for the CCD have not been fully characterized, and are the most likely source of these unidentified features. These X-ray peaks limit the DAMIC reach in a DM search, and point to the need of improving the isotopic control of the apparatus.

The low energy nuclear recoil candidates were selected as described above and the resulting spectrum is shown in Fig. 12. Given the shallow depth of the underground site, we expect that most of the events in the spectrum correspond to neutrons produced from cosmic ray muons hitting the rock or the lead shield. Because of the lack of timing information from CCDs due to the long exposure, DAMIC cannot benefit from an active muon veto as is commonly used in other DM searches. The number of events passing each selection criteria are shown in Table I

## VI. RESULTS AND CONCLUSION

Standard techniques described in Ref. [27] were used to interpret these results as a cross section limit for spin-independent DM interactions. We assume a local WIMP density of 0.3 GeV/cm, dispersion velocity for the halo of 230 km/s, earth velocity of 244 km/s and escape velocity of 650 km/sec. The Lindhard model was used to obtain recoil energies as discussed above. Other possible combinations of parameters could have been used, in particular, the choice of escape velocity might be considered optimistic for this analysis. However, these choices were

made to compare directly with recent publications from experiments looking for low mass dark matter particles [4].

The optimal interval method [34–37] was used for determining the upper limit on DM cross section as a function of mass. The energy range used for this analysis is between 0.05 keVee and 2 keVee as shown in Fig.12. The resulting 90% C.L. limits are shown in Fig. 13, and constitute the new best limit for dark matter particles of masses below 4 GeV. This corresponds to an improvement over the limits produced by CRESST-I [38], which were achieved using sapphire cryogenic detectors with a threshold of 600 eV and exposure of 1.5 kg-day. The region consistent with a DM interpretation of the DAMA/LIBRA signal is shown as a shaded area in Fig. 13, along with recent results from the CoGeNT collaboration interpreted as a DM signal [4, 9]. These two results make the low mass region very interesting and clearly in need of further studies.

The test at the shallow site presented here shows an average background rate of 600 cpd/keV (see Fig. 11). This initial setup did not have a shield for neutrons coming from the rock. Because of the lack of timing information on CCDs, it is not possible to take advantage of an active muon veto to remove cosmogenic neutrons. For these reasons the largest contribution to the background comes from neutrons. The next step for this technology becomes then the development of a CCD experiment in a deeper site (where cosmogenic neutrons become negligible) and with an efficient neutron shield. A CCD search for DM with a background of 10 cpd/keV and a threshold of 40 eVee would improve the limit presented here by a factor of 60, and could provide a new probe for the low mass region where hints of DM have been observed by other experiments. The DAMIC collaboration is currently considering an installation of the experiment at SNOLAB to reach this goal.

Recently we have demonstrated that 0.2 e- R.M.S. readout noise can be achieved with a new type of CCD detector fabricated by LBNL using the same high-resistivity Si technology [42], but with a non-destructive output circuit enabling multiple readouts to reduce noise, a so-called "skipper CCD" [24]. This corresponds to a readout noise 0.72 eV and a reduction of a factor of ten compared to the results presented here. A DM search with the skipper CCD would improve significantly the reach at low energies and is being considered as part of a DAMIC upgrade.

## Acknowledgments

We thank the Fermilab technical staff for their vital contributions, specially: Kevin Kuk, Ken Schultz, Andrew Lathrop, Rolando Flores and Jim Tweed. This work was supported by the U.S. Department of Energy. We thank to FIUNA and CONACyT in Paraguay for their support.

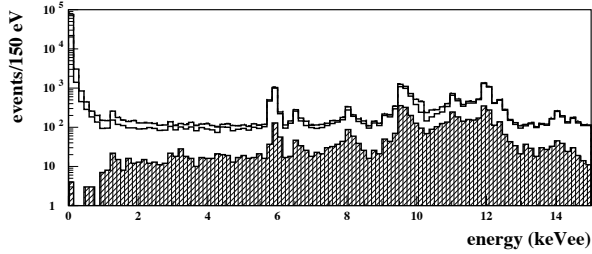


FIG. 11: Energy spectrum for nuclear recoil candidates measured in a 107 g-day exposure for DAMIC. The upper histogram shows the spectrum for all hits, the solid line just below is the result of eliminating the single pixel hits, and the hatched histogram corresponds to the events passing the selection cuts described in the text. The 8.0 keV peak can be attributed to Cu  $K_{\alpha}$  X-rays from the material surrounding the CCD. The 5.9 keV and 6.4 keV peaks can be attributed to the Mn  $K_{\alpha}$  X-rays most likely from cosmogenic  $^{55}\text{Fe}$ . The 9.6 keV peak matches the Au  $L_{\alpha}$  line. The peaks at 11 keV, 12 keV and 14.0 keV match Ge, Br and Sr X-rays, but these elements can not be attributed to any known component in the DAMIC apparatus.

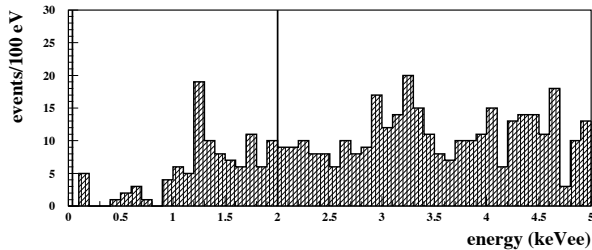


FIG. 12: Low energy spectrum of events passing the selection cuts. The vertical lines at 0.04 keV and 2 keV show the energy range used for the DM analysis.

- 
- [1] The CDMS II Collaboration, *Science*, Vol. 327. no. 5973, pp. 1619 - 162; Aprile E., Doke T., *Reviews of Modern Physics*, Volume 82, July-September (2010); Angle J., et al. (XENON Collaboration), *Phys. Rev. D* 80, 115005 (2009); Broniatowski A., et al. - *Phys. Lett. B* 681 (2009), 305-309 (arXiv:0905.0753); Sanglard V., et al. - *Phys. Rev. D* 71:122002,2005 (astro-ph/0503265); Behnke E., et al, *Science* 15 February 2008.
- [2] B. W. Lee and S. Weinberg, *Phys. Rev. Lett.* , **39** 165 (1977); Murayama, Lectures at Les Houches Summer School, Session 86, Particle Physics and Cosmology: the Fabric of Spacetime, July 31- August 25, 2006, arXiv:0704.2276v1
- [3] Bernabei R. et al., "New results from DAMA/LIBRA", (arXiv:1002.1028) *Eur. Phys. J. C* 67 (2010) 39; Bernabei R. et al., "The DAMA/LIBRA apparatus", *Nucl. Instr. & Meth. A* 592 (2008) 297 (arXiv:0804.2738); Bernabei R., et al., First results from DAMA/LIBRA and combined results with DAMA/NaI, *Eur. Phys. J. C* 56 (2008) 333-355 (arXiv:0804.2741)
- [4] *Physical Review Letters*, vol. 107, Issue 14, id. 141301 (2011); *Physical Review Letters*, vol. 106, Issue 13, id. 131301; *Physical Review Letters*, vol. 101, Issue 25, id. 251301 (2008)
- [5] A. Bottino, F. Donato, N. Fornengo and S. Scopel, *Phys. Rev. D* 69, 037302 (2004) [hep-ph/0307303]
- [6] A. Bottino, F. Donato, N. Fornengo and S. Scopel, *Phys. Rev. D* 81, 107302 (2010) [arXiv:0912.4025]

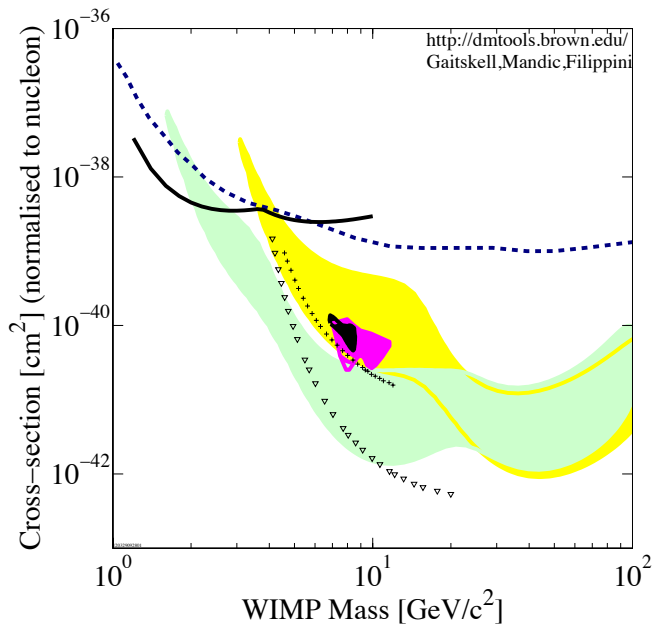


FIG. 13: Cross section upper limit at 90% C.L. for the DAMIC results (solid black) compared to CRESST 2001 (dashed blue), XENON10 [40] (triangles) and CDMS [41] (crosses). The shaded areas correspond to the 5-sigma contour consistent with the DAMA/LIBRA annual modulation signal (yellow: no ion channeling, green: ion channeling) [39]. The magenta contour corresponds to the DM interpretation of the CoGent observed excess and the black contour is the region of interest for the CoGent annual modulation signal [4].

[7] N. Fornengo, S. Scopel and A. Bottino, Phys. Rev. D 83, 015001 (2011) [arXiv:1011.4743]  
 [8] Fitzpatrick A.L., Physical Review D, vol. 81, Issue 11, id. 115005 [arXiv:1003.0014]  
 [9] Hooper, D.; Collar, J.I.; Hall, Jeter; McKinsey, Dan Physical Review D, vol. 82, Issue 12, id. 123509 [arXiv:1007.1005]  
 [10] Frandsen M.T., Sarkar S., PRL 105 (2010) 011301 [arXiv:1003.4505]  
 [11] Cohen, T.; Phalen, D.J.; Pierce, A.; Zurek, K.M., Physical Review D, vol. 82, Issue 5, id. 056001 [arXiv:1005.1655]  
 [12] Cui, Yanou et al, Journal of High Energy Physics, Issue 05, pp. 076 (2009).  
 [13] P.S. Barbeau, J.I. Collar and O. Tench, Journal of Cosmology and Astroparticle Physics, 09 009 (2007).  
 [14] S.E. Holland, D.E. Groom, N.P. Palaio, R. J. Stover, and M. Wei, IEEE Trans. Electron Dev., 50 225 (2003),

LBNL-49992.  
 [15] SNAP Collaboration, G. Aldering *et al.*, Publ. Astr. Soc. Pac., astro-ph/0405232; SNAP Collaboration, astro-ph/0507459.  
 [16] M. Satoshi et al., Ground-based and Airborne Instrumentation for Astronomy. Edited by McLean, Ian S.; Iye, Masanori. Proceedings of the SPIE, Volume 6269, (2006)  
 [17] Flaughner, B., Ground-based and Airborne Instrumentation for Astronomy. Edited by McLean, Ian S.; Iye, Masanori. Proceedings of the SPIE, Volume 6269, (2006)  
 [18] Dark Energy Survey Collaboration, astro-ph/0510346.  
 [19] J. Estrada & R. Schmidt, Scientific Detectors for Astronomy 2005, Edited by J.E. Beletic, J.W. Beletic and P. Amico, Springer, (2006).  
 [20] J. Estrada et al., Ground-based and Airborne Instrumentation for Astronomy. Edited by McLean, Ian S.; Iye, Masanori. Proceedings of the SPIE, Volume 6269, (2006).  
 [21] H.T. Diehl et al., High Energy, Optical, and Infrared Detectors for Astronomy III, Edited by David A. Dorn and Andrew D. Holland. Proceedings of the SPIE, Volume 7021 (2008).  
 [22] D.N. Philip, N.C. Buchholz; Advanced Software, Control, and Communication Systems for Astronomy. Edited by Lewis, Hilton; Raffi, Gianni. Proceedings of the SPIE, Volume 5496, pp. 373-381 (2004), [http://www.noao.edu/ets/new\\_monsoon](http://www.noao.edu/ets/new_monsoon)  
 [23] Estrada et al, Proceedings of the SPIE (2010).  
 [24] J.R. Janesick, Scientific Charge Coupled Devices, SPIE press (2001).  
 [25] H. Cease, H. T. Diehl, J. Estrada, B. Flaughner and V. Scarpine, Experimental Astronomy, Online First (2007)  
 [26] Bertin, E. and Arnouts, S. Astronomy and Astrophysics Supplement 117 393 (1996).  
 [27] J.D. Lewin and P.F. Smith, Astropart. Phys. 6, 87 (1996).  
 [28] J. Lindhard, V. Nielsen, M. Scharff, and P.V. Thomsen, Mat. Fys. Medd. Dan. Selsk 33, 10 (1963).  
 [29] Chagani, H et al, Measurement of the quenching factor of Na recoils in NaI(Tl), 2008 JINST 3 P06003  
 [30] <http://geant4.web.cern.ch/geant4/>  
 [31] <http://cryomech.com>  
 [32] <http://www-numi.fnal.gov/PublicInfo/forscientists.html>  
 [33] E. Behnke, Phys. Rev. Lett. 106, 021303 (2011)  
 [34] HDMS, L. Baudis et al., Phys. Rev. D 59 (1999) 022001.  
 [35] IGEX, A. Morales et al., Phys. Lett. B 489 (2000) 268.  
 [36] ROSEBUD, S. Cebrian et al., Astropart. Phys. 15 (2001) 79  
 [37] EDELWEISS, A. de Bellefon et al., Astropart. Phys. 6  
 [38] G. Angloher et al, Astroparticle Physics 18 (2002) 4355 as interpreted in Savage et al., arXiv:0808.3607v2 ( Fig. 11)  
 [40] J. Angle et al, Phys.Rev.Lett.107:051301,2011  
 [41] CDMS collaboration, Phys.Rev.Lett.106:131302,2011  
 [42] G. Moroni et al, arXiv:1106.183 (2011).